Plant Molecular Biology (2019) 101:455–469
https://doi.org/10.1007/s11103-019-00916-9

Comprehensive survey of the VxGΦL motif of PP2Cs from *Oryza sativa* reveals the critical role of the fourth position in regulation of ABA responsiveness

Seungsu Han[1] · Ji-young Lee[2] · Yeongmok Lee[1] · Tae-Houn Kim[2] · Sangho Lee[1]

Received: 2 May 2019 / Accepted: 4 September 2019 / Published online: 20 September 2019

Abstract

Regulation of abscisic acid (ABA) signaling is crucial in balancing responses to abiotic stresses and retaining growth in planta. An ABA receptor (PYL/RCAR) and a protein phosphatase (PP2C), a co-receptor, form a complex upon binding to ABA. Previously we reported that the second and fourth positions in the VxGΦL motif of PP2Cs from *Oryza sativa* are critical in the interaction of PP2Cs with PYL/RCARs. Considering substantial effects of the VxGΦL motif on ABA signaling outputs, further comprehensive characterization of residues in the second and fourth positions are required. Here we surveyed the second and fourth positions of the VxGΦL motif by combination of biochemical, structural and physiological analyses. We found that the fourth position of the VxGΦL motif, highly conserved to small hydrophobic residues, was a key determinant of the OsPP2C50:OsPYL/RCAR interactions across subfamilies. Large hydrophobic or any hydrophilic residues in the fourth position abrogated ABA responsiveness. Analysis of crystal structures of OsPP2C50 mutants, S265L/I267V ("LV"), I267L ("SL") and I267W ("SW"), in complex with ABA and OsPYL/RCAR3, along with energy calculation of the complexes, uncovered that a bulky hydrophobic residue in the fourth position of the VxGΦL motif pushed away side chains of nearby residues, conferring side-chain rotameric energy stress. Hydrophilic residues in this position imposed solvation energy stress to the PP2C:PYL/RCAR complex. Germination and gene expression analyses corroborated that OsPP2C50 AS and AK mutants modulated ABA responsiveness in *Arabidopsis*. Our results suggest that ABA responsiveness could be fine-tuned by the fourth position of the VxGΦL motif on PP2Cs.

Key message **We comprehensively surveyed the VxGΦL motif to find that the fourth position, highly conserved to small hydrophobic residues, was critical in regulating ABA responsiveness.**

Keywords ABA signaling · ABA receptor · Type 2C protein phosphatase · VxGΦL motif · *Oryza sativa*

Introduction

Abscisic acid (ABA), a phytohormone, employs abiotic stress tolerance of plants. Drought, high salinity and cold trigger biosynthesis of ABA and increase its cellular level, thereby initiating ABA signaling transduction leading gene expression and physiological responses (Cutler et al. 2010; Finkelstein 2013; Rabbani et al. 2003; Seki et al. 2002). The core signaling network of ABA pathway consists of three protein classes: soluble ABA receptors PYL/RCAR (pyrabactin resistance/pyrabactin resistance-like/regulatory component of ABA receptor), ABA co-receptor clade A PP2C (clade A type-2C protein phosphatase) and signaling effector SnRK2 (sucrose non-fermenting1-related protein kinase 2) (Cutler et al. 2010). Under normal states at low ABA level in cytoplasm, PP2C interacts with SnRK2,

Electronic supplementary material The online version of this article (https://doi.org/10.1007/s11103-019-00916-9) contains supplementary material, which is available to authorized users.

✉ Sangho Lee
sangholee@skku.edu

[1] Department of Biological Sciences, Sungkyunkwan University, Suwon 16419, Republic of Korea

[2] Department of Prepharm-Med/Health Functional Biomaterials, Duksung Women's University, Seoul 01369, Republic of Korea

leading to functional inactivation of SnRK2 by dephosphorylating its activation loop and spatial blocking to its active site (Soon et al. 2012; Vlad et al. 2009; Zhou et al. 2012). Under abiotic stress situations, ABA accumulation occurs and PYL/RCAR and its co-receptor PP2C recognize ABA to form a receptor:co-receptor complex. This results in release of SnRK2 from PP2C and self-activation by activation loop autophosphorylation (Ng et al. 2011). Then, SnRK2 gains its functional activity and exerts signaling to downstream.

Clade A PP2C functions as a negative regulator in the ABA signaling pathway with two motifs for interactions with other core ABA components: the wedging tryptophan residue and the VxGΦL motif (Han et al. 2017; Melcher et al. 2009; Saez et al. 2004; Soon et al. 2012). Both PYL/RCAR and SnRK2 interact with PP2C through these motifs, providing structural basis for "binding mimicry" (Han et al. 2017; Soon et al. 2012). The wedging tryptophan is highly conserved among clade A PP2Cs and its detailed role in mediating the interaction with PYL/RCAR and SnRK2 has been established (Melcher et al. 2009; Soon et al. 2012). Structurally, the wedging tryptophan mediates the interaction with PYL/RCAR and SnRK2 by wedging itself into the binding cleft and participates in recognition of ABA with PYL/RCAR. $N\varepsilon_1$ of the wedging tryptophan stabilizes ABA by water-mediated hydrogen bonds (Melcher et al. 2009). The same wedging tryptophan is also inserted into catalytic cleft of SnRK2 to mimic PP2C:PYL/RCAR interaction. This interaction effectively suppresses the activity of SnRK2 by steric hindrance (Soon et al. 2012). Consistent with the structural analysis, the wedging tryptophan mutant of clade A PP2C, such as AtHAB1 W385A, showed ABA insensitive physiology in Arabidopsis (Dupeux et al. 2011). Another interacting motif, the VxGΦL motif (Han et al. 2017), is adjacent to the conserved wedging tryptophan of clade A PP2Cs. Its second and fourth positions are usually conserved to aliphatic residues, yielding the consensus sequence being 'VLGVL' in seed plants, such as Arabidopsis, rice and maize (Supplementary Fig. S1). Sequence alterations of these two residues to hydrophilic amino acid, such as lysine, are detrimental to PP2C:PYL/RCAR interaction. When these sequences were changed to several natural variants, the binding affinities between OsPP2C50 mutants and OsPYL/RCAR3 decreased. For example, the motif with 'VFGML' sequence in OsPP2C50 showed about 15-fold weaker binding affinity to OsPYL/RCAR3 than its wild-type. Similar to wedge tryptophan, alteration of the VxGΦL motif also influences the interaction with a kinase. Mutations of this motif of OsPP2C50 lead to functional inactivation and steric inhibition of SAPK10, a rice kinase (Han et al. 2017). Taken together, clade A PP2Cs are critical in ABA signaling pathway, thereby rendering plants more tolerant to abiotic stresses including drought.

Here, we comprehensively surveyed effects of the second and fourth positions of the VxGΦL motif on the interaction of a PP2C with a PYL/RCAR and phenotypes of PP2C-OX transgenic plants by integrating structural, biochemical and physiological analyses. We found that ABA responsiveness mediated by PP2C:PYL/RCAR complex could be modulated by the fourth position of the VxGΦL motif. This position preferred aliphatic residues in terms of interaction with PYL/RCAR. Thus, ABA responsiveness could be modulated by placing large hydrophobic or any hydrophilic residues in the fourth position. Based on structural analysis and energy calculation of PP2C:PYL/RCAR complexes, we provided a framework to understand how aliphatic residues in the fourth position contribute to PP2C:PYL/RCAR complex stability. We finally introduced OsPP2C50 mutants into *Arabidopsis* and found that some mutant likes could possibly modulate ABA signaling pathway, validating in vitro findings.

Methods

Cloning and site-directed mutagenesis

We utilized the plasmids used in previous paper (Han et al. 2017). We generated additional mutants by QuikChange site-directed mutagenesis methods (Agilent), using *Pfu* polymerase (Solgent) and *Dpn* I (New England Biolabs). We verified identities of all mutants by DNA sequencing.

Protein expression and purification

Wild type and VxGΦL motif mutants of OsPP2C50 as GST fusion proteins and OsPYL/RCAR3, 5, 9 and 10 as 6xHis tagged proteins were expressed and purified following the method as described previously (Han et al. 2017). Briefly, Rosetta2(DE3) cells (Novagen) containing plasmids encoding OsPP2C50 and OsPYL/RCARs were cultured in LB media, induced with 0.1 mM IPTG, and further grown for 5 h at 16 °C with gentle shaking. GST-OsPP2C50 proteins and His-OsPYL/RCAR3, 5, 9 and 10 were purified by affinity chromatography using glutathione-Sepharose 4B resin (GE HealthCare) and Ni–NTA resin (Qiagen), respectively. Proteins were finally dialyzed to final storage buffer (20 mM Tris–HCl pH 8.0, 200 mM NaCl, 0.1 mM TCEP and 10% (v/v) glycerol) and frozen at − 80 °C, which was supplemented with 1 mM $MgCl_2$ to GST-OsPP2C50 proteins.

6xHis tagged OsPYL/RCAR1 and 8, both of which were not used in the previous study (Han et al. 2017), were expressed as predominantly insoluble inclusion bodies. Subsequently, OsPYL/RCAR1 and 8 were refolded by freeze-and-thaw method in weak chaotropic agent condition (Qi et al. 2015). Rosetta2(DE3) was transformed by plasmids encoding 6xHis tagged OsPYL/RCAR1 and 8 and

overexpressed by 0.1 mM IPTG induction followed by subsequent culture for 3 h at 37 °C. After cell lysis by ultrasonication and centrifugation, pellets were collected and washed by pellet wash buffer (50 mM Tris–HCl pH 8.0, 100 mM NaCl, 1 mM EDTA, 1% (v/v) triton X-100 and 1 M urea). Washed pellets were resuspended to denaturing buffer (20 mM Tris–HCl pH 8.0, 200 mM NaCl, 0.1 mM TCEP and 2 M Urea), frozen at − 20 °C and thawed at room temperature. After centrifugation to remove pellets not denatured completely, supernatants were collected and dialyzed to purification buffer (20 mM Tris–HCl pH 8.0, 200 mM NaCl and 0.1 mM TCEP) and performed purification steps using Ni–NTA resin described previously. All purified proteins were validated by SDS-PAGE.

GST pull-down assay and western blot

We employed purified GST-PP2C50 wild-type, S265K (KI mutant), I267K (SK mutant) and S265K/I267K (KK mutant) as baits for GST pull-down assay. These bait proteins were also used in the previous study (Han et al. 2017). Firstly, 5 µg of GST-PP2C proteins were added to pull-down buffer (20 mM Tris–HCl pH 8.0, 1 mM $MgCl_2$, 0.1 mM TCEP, 0.1 mg/ml BSA, 0.1% (v/v) NP-40 and 0.1 mM ABA) with pre-washed glutathione-Sepharose resin (GE HealthCare). For binding of the bait proteins to the resin, we incubated at room temperature for 2 h with gentle agitation. Next, 5 µg of purified His-OsPYL/RCAR1, 3, 5, 8, 9 and 10 were added as prey proteins with additional incubations for 2 h. We washed the incubated resins by pull-down buffer three times and eluted proteins by the same buffer with 10 mM reduced glutathione. Then, we performed SDS-PAGE and western blot with anti-His and anti-GST antibodies (Santa Cruz).

Phosphatase assay

We followed the method in ABA dependent manner as described previously (Han et al. 2017). Briefly, 80 nM of GST-PP2C50 wild-type and mutants and 400 nM of His-OsPYL/RCAR3 were added in phosphatase assay buffer (20 mM Tris–HCl pH 8.0, 1 mM $MnCl_2$, 0.1% (v/v) 2-Mercaptoethanol and 0.1 mg/ml BSA) containing various concentrations of ABA. After pre-incubation for 10 min at 37 °C, phosphatase assay was started by adding 15 mM (final concentration) of pNPP (*p*-nitrophenyl phosphate) as a substrate of GST-PP2C50 s. After incubation for 1 h at 37 °C, the amount of *p*-nitrophenol was determined by absorbance at 405 nm. OsPP2C50 s' IC_{50} value was calculated by *Prism 5* (GraphPad Software, Inc.) using the following equation:

$$y = \frac{100}{\left(1 + 10^{(x - \log IC50)}\right)}$$

where x and y refer to relative phosphatase activity (%) and log scale of ABA concentration (µM), respectively.

Biolayer interferometry (BLI) assay

We performed biolayer interferometry assay on a BLItz system with anti-GST biosensors (ForteBio) as described previously (Han et al. 2017). All buffers containing purified proteins were exchanged to BLI assay buffer (20 mM Tris–HCl pH 8.0, 200 mM NaCl, 5 mM $MgCl_2$, 0.1 mM TCEP, 0.05% (v/v) Tween 20, 1 mg/ml BSA and 0.1 mM ABA). Firstly, 25 µg of GST-OsPP2C50 proteins were immobilized to the sensors and washed by the BLI assay buffer. Next, the sensors were reacted with 0.5 µM of His-OsPYL/RCAR3 for association steps and washed by the BLI assay buffer for dissociation buffer. All sensograms were corrected with the reference signal, which was measured with BLI assay buffer without any proteins for association and dissociation steps. We calculated association rate constant (k_{on}), dissociation rate constant (k_{off}) and their standard error of the mean (S.E.M.) using BLItz Pro (ForteBio). Dissociation constants (K_D) were calculated by the following equation:

$$k_D = k_{off} / k_{on}$$

and SEM of dissociation constants were induced by the following equation:

$$\frac{\Delta K_D}{K_D} = \sqrt{\left(\frac{\Delta k_{on}}{k_{on}}\right)^2 + \left(\frac{\Delta k_{off}}{k_{off}}\right)^2}$$

where Δ refers to SEM of K_D, k_{on} and k_{off}, respectively. The R^2 analysis, which is an indication of goodness of graph curve fitting, was performed by *BLItz Pro*, and the R^2 values of all experiments were above 0.98.

Directed evolution of the VxGΦL motif of OsPP2C50

Firstly, we performed NNK-primer based random mutagenesis on the second and fourth positions of the VxGΦL motif of OsPP2C50, respectively. Randomly generated mutations were confirmed by Sanger DNA sequencing method. *E. coli* was transformed by plasmids encoding GST-OsPP2C50 with its mutated VxGΦL motif. These cells were spread onto agar LB plate containing antibiotics for transformed cell selection. Each colony was transferred into LB media separately in each well of a 96-well plate for protein overexpression. Next, cells were harvested by centrifugation and lysed by T4 lysozyme treatment. The cell lysate was transferred to a new 96-well plate coated by His-OsPYL/RCAR3 and incubated with (+)-ABA into buffer. The lysate was discarded and washed, and then we detected how well each GST-OsPP2C50 mutant interacted with OsPYL/RCAR3 using

HRP-conjugated anti-GST antibody with TMB treatment as a substrate of HRP. Top 10 wells showing higher signals than mean plus S.D. of bound GST-OsPP2C50 wild-type signals were analyzed by DNA sequencing.

Protein crystallization

OsPP2C50 (58–387) E139A/E140A/K142A served as the "wild-type" (Han et al. 2017) for crystallization with OsPYL/RCAR3 and ABA. For protein crystallization, protein complexes OsPYL/RCAR3:ABA with OsPP2C50 S265L/I267V (LV mutant), I267L (SL mutant) and I267W (SW mutant) were purified by Ni–NTA affinity chromatography, ion-exchange chromatography and size-exclusion chromatography as described previously (Han et al. 2017). The protein complexes of LV mutant, SL mutant and SW mutant were concentrated to 11.5 mg/ml, 8.8 mg/ml and 8.7 mg/ml, respectively. To check probabilities of protein crystallization, we measured the polydispersity of the concentrated protein complex samples by dynamic light scattering on a DynaPro NanoStar (Wyatt). The complex protein crystals were grown at 22 °C by hanging drop method where 2 µl of the purified complex protein was mixed with 2 µl of reservoir solutions. The optimized reservoir conditions yielding the best crystals were 7.5% (w/v) PEG3350 and 80 mM ammonium thiocyanate of LV mutant complex, 12% (w/v) PEG8000, 100 mM MES pH 6.0 and 300 mM magnesium acetate of SL mutant complex and 15% (w/v) PEG3350, 130 mM sodium thiocyanate and 300 mM glycine. All crystals appeared within 2 days and grew to the maximum size within 6 days.

Crystallographic data collection and structure determination

We flash froze crystals at 100 K in liquid nitrogen gas stream with addition of 15% (v/v) glycerol as cryoprotectant. Then, we collected the diffraction data using a Quantum 315r CCD detector (ADSC) at beamline 5C of Pohang Accelerator Laboratory (PAL). We performed data processing, reduction and scaling using *HKL2000* (Otwinowski and Minor 1997). We determined the complex protein structures by molecular replacement using *PHASER-MR* of the *PHENIX* suite (Adams et al. 2010) with OsPP2C50:ABA:OsPYL/RCAR3 (PDB ID: 5GWP) (Han et al. 2017) as an initial search model. We fitted models manually using *COOT* (Emsley and Cowtan 2004), and performed model refinement by *PHENIX* refinement. The data collection and refinement statistics of structures are summarized in Supplementary Table S1. All protein structure figures were produced by *PyMOL* (Schrödinger).

Protein structural energy calculation and analysis in silico

We performed all energy calculations and analysis with *Rosetta 3* suite. Structural for all the mutants were generated by in silico mutagenesis using OsPP2C50:OsPYL/RCAR3 wild-type structure as a reference model (PDB ID: 5GWP). Firstly, we performed Relax protocol which relieved clashes in the given structural models and prepared the relaxed models for energy scoring (Conway et al. 2014). To calculate per-residue-energy and determine the contributions of residues to OsPP2C50:OsPYL/RCAR3 interaction, energy scoring with score function REF2015 was performed using per_residue_energies protocol (O'Meara et al. 2015).

Generation of *Arabidopsis* transgenic lines expressing *OsPP2C50* mutants

Full length cDNA of *OsPP2C50* wild-type and its mutants were cloned into pENTR/D-TOPO (Invitrogen) and integrated into the pH35GS binary vector through GATEWAY LR reaction using Lambda Integrase/Excisionase (ELPis). Subsequently, *Agrobacterium tumefaciens* strain GV3101 mediated transformation of 6-week-old wild-type Col-0 by floral-dip method to generate 35S promoter-driven *OsPP2C50-OX* transgenic lines (Clough and Bent 1998). 14 to 35 T1 plants of *OsPP2C50-OX* wild-type and mutant lines were selected on half-strength MS (Murashige and Skoog) media containing 8 mg/L hygromycin. 9 to 10 T2 plants from each T1 line were tested on hygromycin media to select homozygous transgenic overexpression lines.

ABA sensitivity analyses of seed germination and primary root growth assay

For seed germination assay, 30 seeds of each transgenic line expressing *OsPP2C50-OX* wild-type and mutants were sterilized and sowed on half-strength MS agar media containing 0 µM (control) or 0.5 µM ABA. 2 days after vernalization at 4 °C, the media were transferred to a growth chamber maintained at a 22 °C, long-day condition. The germination rate of each transgenic line was examined daily. For primary root growth assay, Col-0 seedlings and *OsPP2C50-OX* transgenic lines were vertically grown on half-strength MS agar media for 10 days and transferred to a new MS agar medium in the presence of 10 µM ABA. The lengths of the primary root additionally grown on the new medium for 6 days were measured. Triplet data were obtained by three experiments independently.

ABA treatment and gene expression analyses by quantitative real-time PCR

Col-0 and *OsPP2C50-OX* lines were grown in half-strength MS agar media vertically for 7 days and treated with 10 µM ABA or control solution for 6 h. Total RNA of each plant sample was extracted using TRIzol reagent (Bioline). 2 µg of the total RNA was used for cDNA synthesis using SensiFAST cDNA synthesis kit (Bioline). 1.5 µl of each cDNA template was included in 15 µl of total quantitative RT-PCR reaction mixture. SensiFAST™ SYBR Hi-ROX kit (Bioline) and StepOnePlus real-time PCR system (Applied Biosystems) were utilized for gene expression analyses. All experiments were repeated three times, and the primers used in this experiment are listed in Supplementary Table S4.

Results

Residue in the fourth position of the VxGΦL motif is the crucial determinant for OsPP2C50:OsPYL/RCAR3 interactions

Previously we reported the new conserved region of the PP2C protein, the VxGΦL motif, which mediated hydrophobic interaction with ABA receptors in presence of ABA (Han et al. 2017). The second and fourth residues of the VxGΦL motif of the PP2C are juxtaposed to the ABA receptor. To systematically interrogate the effects of these residues on the interaction with the ABA receptor, we performed glutathione *S*-transferase (GST) pull-down assay using GST-OsPP2C50 and six of His-OsPYL/RCARs: OsPYL/RCAR3, 5 and 8 in subfamily I, OsPYL/RCAR1 in subfamily II, and OsPYL/RCAR9 and 10 in subfamily III (Kim et al. 2012; Tischer et al. 2017). Since the second and fourth residues of the VxGΦL motif were predominantly occupied by nonpolar residues in PP2Cs of *Arabidopsis*, rice and maize (Supplementary Fig. S1, red box), we performed hydrophile scanning in these residues. In the previous study, we observed the engagement of the VxGΦL motif in the interaction with a subset of OsPYL/RCARs (OsPYL/RCAR3, 5, 9 and 10) (Han et al. 2017). To corroborate that the VxGΦL motif is involved in the interactions with all subfamilies of OsPYL/RCARs clearly, the binding affinities with all the subfamilies of OsPYL/RCARs were tested by GST pull-down assay with more stringent condition than in the previous work, with additional detergent (0.1% NP-40) and half the amount of OsPYL/RCARs (5 µg) used (Han et al. 2017). GST pull-down assay showed that mutations of the fourth residue to lysine (SK mutant) were highly detrimental to the interaction between OsPP2C50 and OsPYL/RCARs (Fig. 1a). The double hydrophile mutants of the VxGΦL motif (KK mutant)

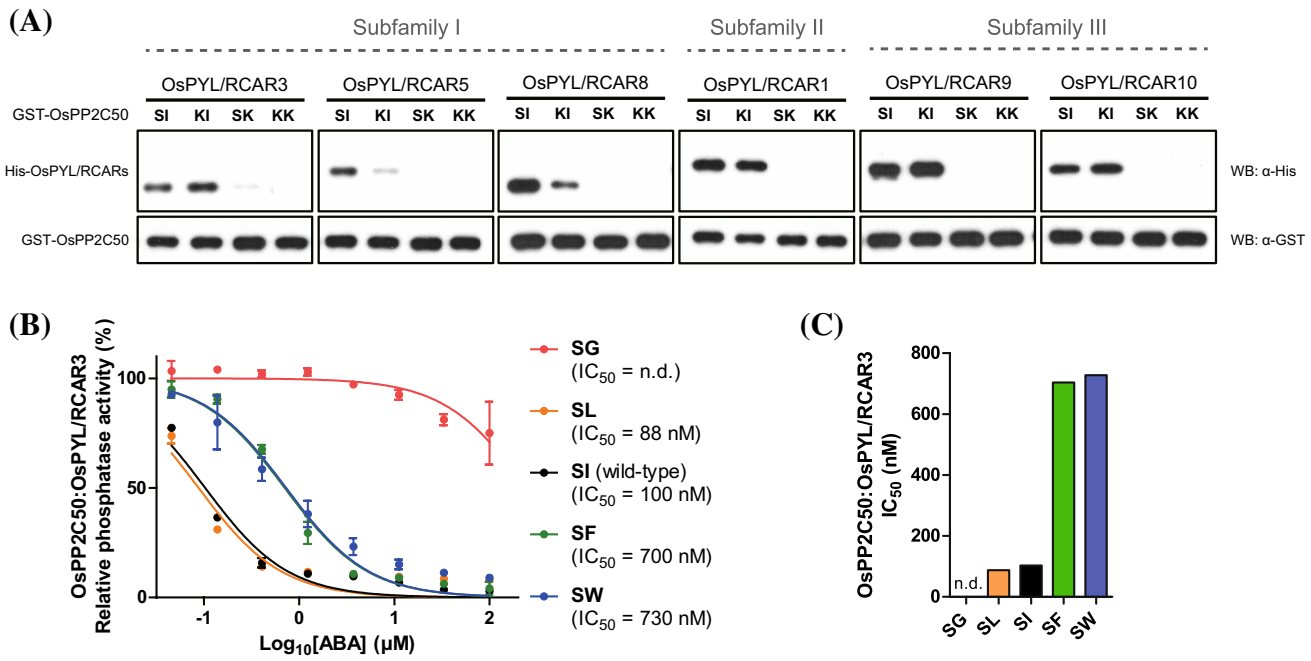

Fig. 1 Characterization of key residues in the VxGΦL motif of OsPP2C50 involved in interaction with OsPYL/RCARs. **a** VxGΦL motif residues critical in the direct interaction of OsPP2C50 with OsPYL/RCAR1, 3, 5, 8, 9 and 10 were determined by the combination of hydrophile scanning using GST pull-down assay. (**b** and **c**) The half maximal inhibitory concentration (IC_{50}) values for the phosphatase activities of the OsPP2C50 mutants varied on forth residue of the motif. The IC_{50} values are displayed in terms of the ABA concentration and reflect the ABA sensitivity of OsPYL/RCARs with OsPP2C50. *n.d.* not determined

completely lost the interaction with all the ABA receptors we investigated. On the other hand, the change of the second residue to lysine (KI mutant) caused negative impact slightly on interactions to OsPYL/RCAR5 and 8, which were classified to subfamily I ABA receptor, but no impact on those to subfamily II and III ABA receptors. These results imply that the second residue of the motif might have sequence tolerance to maintain the interaction with ABA receptors. As we compared between the conserved VxGΦL motifs of clade A PP2C proteins from *Arabidopsis*, rice and maize, the fourth positions were more conserved to small hydrophobic residues, mostly valine, than the second positions (Supplementary Fig. S1). Thus, we confirmed that the fourth position of the VxGΦL motif was highly involved in interactions with OsPYL/RCARs of all subfamilies, rather than the second position of the motif.

Having established the importance of the hydrophobic fourth residue of VxGΦL motif in ABA signaling, we investigated how the size of hydrophobic side chains modulated the interaction of OsPP2C50 with OsPYL/RCAR3: glycine, leucine, isoleucine (wild-type), phenylalanine and tryptophan. Using the five constructs (SG, SL, SI, SF and SW), we determined the half-maximal inhibitory concentrations (IC_{50}) by phosphatase assay (Fig. 1b, c). IC_{50} of PP2C by ABA concentrations could be regarded as the PP2C:ABA receptor affinity and ABA responsiveness. OsPP2C50 SI (wild-type) and SL mutant showed the lowest IC_{50} values, 100 nM and 88 nM, respectively. By contrast, SG mutant, which does not contain any non-hydrogen side chain atom, showed no affinity to OsPYL/RCAR3. Altering fourth residue to bulky ones such as phenylalanine and tryptophan, SF and SW mutants showed ~ 7 times weaker interaction to OsPYL/RCAR3. These results reinforces that small hydrophobic residue on fourth position of the motif is optimized to maintain PP2C:ABA receptor interaction and suggest the possibility to modulate the OsPP2C50-OsPYL/RCAR3 interaction strength through fourth positions of the VxGΦL motif in three levels: very weak (SG mutant), modest (SF and SW mutant) and strong (wild-type and SI mutant) interactions.

PP2C:PYL/RCAR interaction is influenced by size and hydrophobicity in the second and fourth positions of the VxGΦL motif

Initially we hypothesized that the introduction of larger hydrophobic residues to the motif would enforce the interaction due to hydrophobic environment adjacent to the VxGΦL motif (Han et al. 2017). However, the SF and SW mutants in Fig. 1 shows lower binding affinities to OsPYL/RCARs. The FM mutant, reported in the previous study (Han et al. 2017), also showed about 15-fold lowered binding affinity to OsPYL/RCAR3 in comparison of OsPP2C50 wild-type. To examine correlation between PP2C:PYL/RCAR binding affinity and size of side-chain on VxGΦL motif, we performed bio-layer interferometry to monitor binding affinities of OsPP2C50 mutants to OsPYL/RCAR3 in the presence of ABA (Table 1, serine variants). The dissociation constant (K_d) of the wild-type OsPP2C50 with OsPYL/RCAR3 was 3.7 nM in the presence of 0.1 mM (+)-ABA. We mutated Ile267 on OsPP2C50, the fourth residue of the VxGΦL motif, to variable-sized hydrophobic residues such as leucine (SL mutant), threonine (ST mutant) and tryptophan (SW mutant). The SL mutant, OsPP2C50 I267L, showed 1.5 nM of K_d, which is very similar to that of wild-type. Such a similar affinity of the SL mutant to the wild-type is expected given the very similar chemical structure of both side-chains. The ST mutant where highly hydrophobic isoleucine was replaced by less hydrophobic threonine exhibited a marginal decrease in the affinity (K_d of 7.4 nM), corroborating that the hydrophobicity is essential for the fourth residue of the motif. By contrast, the SW mutant where the aliphatic isoleucine was mutated to aromatic tryptophan weakened the interaction between OsPP2C50 and OsPYL/RCAR3 by almost tenfold (K_d of 29 nM). This observation suggests that bulky hydrophobic residues including aromatic ones can impair the interaction. Collectively, these results revealed that the fourth position of the VxGΦL motif prefers hydrophobic residues with small sizes such as aliphatic hydrophobic ones.

Due to its hydrophobic surroundings adjacent to the VxGΦL motif, we hypothesized hydrophilic residues in the motif would impose a negative effect on OsPP2C50:OsPYL/RCAR3 complex formation. As we showed above, the replacement of the fourth residue of the motif with a charged residue, such as lysine (SK mutant), impaired the interactions with all the subfamilies of OsPYL/RCARs (Fig. 1a). We further extended the investigation of the effects of hydrophilic residues on the fourth residue of the motif using the following additional mutants as well as the SK mutant: serine (SS mutant), glutamine (SQ mutant), and glutamate (SE mutant). As measured the interaction strength of them to OsPYL/RCAR3, we confirmed residue substitution of hydrophilic ones generally reduced binding affinities. The SS mutant, showing the strongest affinity out of hydrophilic mutants, was 10 times weaker than the wild-type (K_d of 32 nM vs. 3.7 nM). From serine to glutamine and lysine, the binding affinities were reduced by 3- and 30-fold, respectively. The SE mutant totally lost the binding affinity to OsPYL/RCAR3 in the presence of 0.1 mM ABA. Taken together, these results corroborate that the hydrophobicity in the VxGΦL motif is crucial to ABA responsiveness.

The second position of the VxGΦL motif on OsPP2C50 is serine, a small hydrophilic residue. The same position is typically occupied by hydrophobic residues in other clade A PP2C proteins (Supplementary Fig. S1). Although the

Table 1 Binding affinities of VxGΦL motif mutants of OsPP2C50

OsPP2C50 Mutant[a]	VΦGΦL motif	$k_{on} \pm$ SEM[b] (10^4 M^{-1} s^{-1})	$k_{off} \pm$ SEM[b] (10^{-4} s^{-1})	$K_d \pm$ SEM[b] (nM)	R^{2c}
Serine variants					
SI[d]	VSGIL	3.1 ± 0.05	1.2 ± 0.17	3.7 ± 0.54	0.98
SL	VSGLL	4.4 ± 0.05	0.65 ± 0.10	1.5 ± 0.24	0.99
ST	VSGTL	3.4 ± 0.02	2.5 ± 0.07	7.4 ± 0.21	0.99
SW	VSGWL	3.4 ± 0.02	9.8 ± 0.18	29 ± 0.57	0.99
SS	VSGSL	5.2 ± 0.03	16 ± 0.25	32 ± 0.51	0.99
SQ	VSGQL	5.7 ± 0.03	51 ± 0.32	90 ± 0.75	0.99
SE	VSGEL	n.d.[e]	n.d.	n.d.	–
SK	VSGKL	1.9 ± 0.05	190 ± 0.94	1030 ± 30	0.99
Alanine variants					
AI	VAGIL	2.8 ± 0.02	2.0 ± 0.09	7.2 ± 0.33	0.99
AS	VAGSL	5.6 ± 0.03	18 ± 0.09	32 ± 0.23	0.99
AQ	VAGQL	2.5 ± 0.03	49 ± 0.12	200 ± 2.5	0.99
AK	VAGKL	4.7 ± 0.15	235 ± 2.3	500 ± 16	0.99

[a]Identities of amino acid residues in positions 265 and 267 of OsPP2C50

[b]*SEM* standard error of mean

[c]R^2 refers to an estimate of the goodness of the curve fit between experimental sensograms and the mathematical model of 1:1 binding kinetics. This value close to 1.0 indicates a good curve fitting

[d]Wild-type

[e]Not determined

effects of size and hydrophobicity of residues in the fourth position of the motif on PP2C:PYL/RCAR interaction were established, the effects of non-canonical hydrophilic residues in the second position were not excluded clearly. Thus, we mutated serine in the second position to alanine, the simplest hydrophobic amino acid, and performed BLI experiments. We generated AI, AS, AQ and AK mutants of OsPP2C50 (alanine variants) where we introduced isoleucine, serine, glutamine and lysine in the fourth position, respectively so that we could compare binding affinities of the aforementioned alanine variants with those of serine counterparts: SI, SS, SQ and SK. When we compared K_d values between the mutants with only the second position being different, i.e., SI vs. AI, SS vs. AS, SQ vs. AQ and SK vs. AK, substitution of alanine for serine did not alter the K_d values significantly (Table 1, alanine variants). The AI, AQ and AK mutants showed about twofold difference of binding affinities to their serine counterparts while the AS mutant revealed the essentially identical affinity. The effects of the fourth position among the alanine variants on the binding affinity were consistent with those among the serine counterparts. The degree of decrease in affinities from AI to AS, AQ and AK followed the same trends for the serine counterparts (4-, 27-, and 70-fold decrease for the alanine variants; 9-, 24-, and 280-fold for the serine variants). These results suggested that OsPP2C50 was tolerant to small hydrophilic residue (alanine variants vs. serine variants) in the second position to but not in the fourth position due to about 5–10 fold decrease of binding affinities (SI vs. SS mutant and AI vs. AS mutant).

Directed evolution of the VxGΦL motif yielded the same combination for the second and fourth positions as the wild-type

To explore whether we could obtain a mutant of the VxGΦL motif with a higher affinity than the wild-type of OsPP2C50, we performed directed evolution (Table 2 and Supplementary Fig. S2). Following random mutation of each of the second and fourth positions of the VxGΦL motif (Supplementary Fig. S2A), we determined the affinity of each mutant of OsPP2C50 with OsPYL/RCAR3 in the presence of (+)-ABA using ELISA (Supplementary Fig. S3B and S3C). In this screening, we excluded wild-type residues, previously studied mutants with lowered affinities (Han et al. 2017) and cysteine which could form an unspecific disulfide bond. Except threonine, screened amino acids were hydrophobic rather than hydrophilic or charged ones (Table 2). Combined with multiple sequence alignments of the VxGΦL motif in plants (Supplementary Fig. S1) and structural analysis about hydrophobic surroundings adjacent to the VxGΦL motif (Fig. 2 and previous report (Han et al. 2017)), the results from directed evolution supported that the VxGΦL motif prefers hydrophobic residues to polar or charged ones and that hydrophobic residues in the motif

Table 2 The motif sequence of the directed evolution clones analyzed by DNA sequencing

Clone	Motif sequence	Result[a]	Note
SSM: VXGΦL			
A1	VSGIL	–	Wild-type
C3	VAGIL	+	
D3	VCGIL	–	Probably interaction by disulfide bond[b]
E9	VSGIL	–	Wild-type
SSM: VXGΦL			
A3	VSGLL	+	
A4	VSGVL	–	Han et al. (2017)[c]
A7	VSGCL	–	Probably interaction by disulfide bond
B5	VSGLL	+	
B6	VSGWL	+	
B8	VSGTL	+	
B10	VSGCL	–	Probably interaction by disulfide bond
B12	VSGCL	–	Probably interaction by disulfide bond
C2	VSGVL	–	Han et al. (2017)
D11	VSGCL	–	Probably interaction by disulfide bond

[a]Positive results indicates promising candidates showing higher affinities than OsPP2C50 wild-type

[b]Mutations to cysteine were rejected as engineered candidates due to the probability of false positive induced by disulfide bonds

[c]Mutants previously studied (Han et al. 2017) showing lower affinities than wild-type were also rejected, which is described on 'Note' column

would optimize OsPP2C50 for its ABA responsiveness with OsPYL/RCAR3.

Crystallographic analysis of the VxGΦL motif mutants supports preference of aliphatic residues in the fourth position of the VxGΦL motif

To elucidate how size of fourth position of the motif could determine the interaction strength in molecular level, we determined the crystal structures of OsPP2C50 LV, SL and SW mutants complexed with ABA and OsPYL/RCAR3 (Fig. 2 and Table 3). Since the consensus sequence of the VxGΦL motif was VLGVL, we generated the LV mutant. The SL and SW mutants were selected because they showed the highest and lowest binding affinities among variable-sized hydrophobic mutants. There was no significant difference in the interfaces surrounding the VxGΦL motif as well as overall structures of the wild-type (SI), LV, SL and SW mutants (Fig. 2a, b). Ala177 and Leu178 from OsPYL/RCAR3 and Try278, Leu279 and the VxGΦL motif from OsPP2C50 constituted a hydrophobic network at the PP2C:PYL/RCAR interface (Fig. 2c). Aliphatic side-chains in the fourth position of the VxGΦL motif, such as Ile267 of wild-type, Val267 of LV mutant and Leu267 of SL mutant, stabilized the hydrophobic interactions at the PP2C:PYL/RCAR interfaces (Fig. 2c: LV, SI and SL). By contrast, in the SW mutant where Trp267 was introduced in the fourth position of the VxGΦL motif, adjacent Tyr278 was pushed away from Leu279 due to bulkier side-chain of Trp267 (Fig. 2c: SW). Conformational simulation of the 267th residue of OsPP2C50 mutants indicated that van der Waals bumps between atoms occurred only in the SW mutant (Supplementary Fig. S3), implicating that the SW mutant would destabilize the binding interface. It seems that aliphatic amino acids in the fourth position of the VxGΦL motif stabilize the OsPYL/RCAR3:ABA:OsPP2C50 complex formation while introduction of tryptophan destabilizes it.

Van der Waals force, side-chain rotamer energy and solvation energy underlie ABA responsiveness alteration through the VxGΦL motif

To obtain further insights in the effects of mutations in the second and fourth positions of the VxGΦL motif, we implemented in silico energy analysis by calculating per-residue energy scores of each mutant complex structure, with particular focus on the 265th and 267th residues of OsPP2C50 corresponding to the second and the fourth positions of the VxGΦL motif (Fig. 3 and Supplementary Tables S1 and S2). We used the crystal structures of the wild-type (SI) and two mutants (SL and SW) and in silico mutated structures of other mutants (SG, ST, SF, SS, SQ, SE, SK, AI, AS, AQ and AK) in which no crystal structures were available. For energy calculations, we employed local structure optimization to relieve clash stresses in given structures by Relax protocol (Conway et al. 2014). In the in silico per-residue energy analysis, a lower energy score value of a residue would indicate that the residue is thermodynamically more stable.

The second position of the motif, the 265th residue of OsPP2C50, had no significant differences between wild-type (SI) and AI mutant in terms of energy score on the residue (Supplementary Table S1). By contrast, the fourth position of the motif, the 267th residue of OsPP2C50, preferred the wild-type (SI) to all other fourth position mutants (SG, SL, ST, SF, SW, SS, and SQ) (Fig. 3a, b serine variants and Supplementary Table S2). Notably, the SL mutant showed the closest energy score to that of the wild-type (SI), corroborating that isoleucine and leucine in the fourth position, having similar size and hydrophobicity, contribute to the stability of the PP2C:PYL/RCAR complex interchangeably (Fig. 3a). The energy scores of the SG, SF and SW mutants significantly increased in comparison to that of the wild-type,

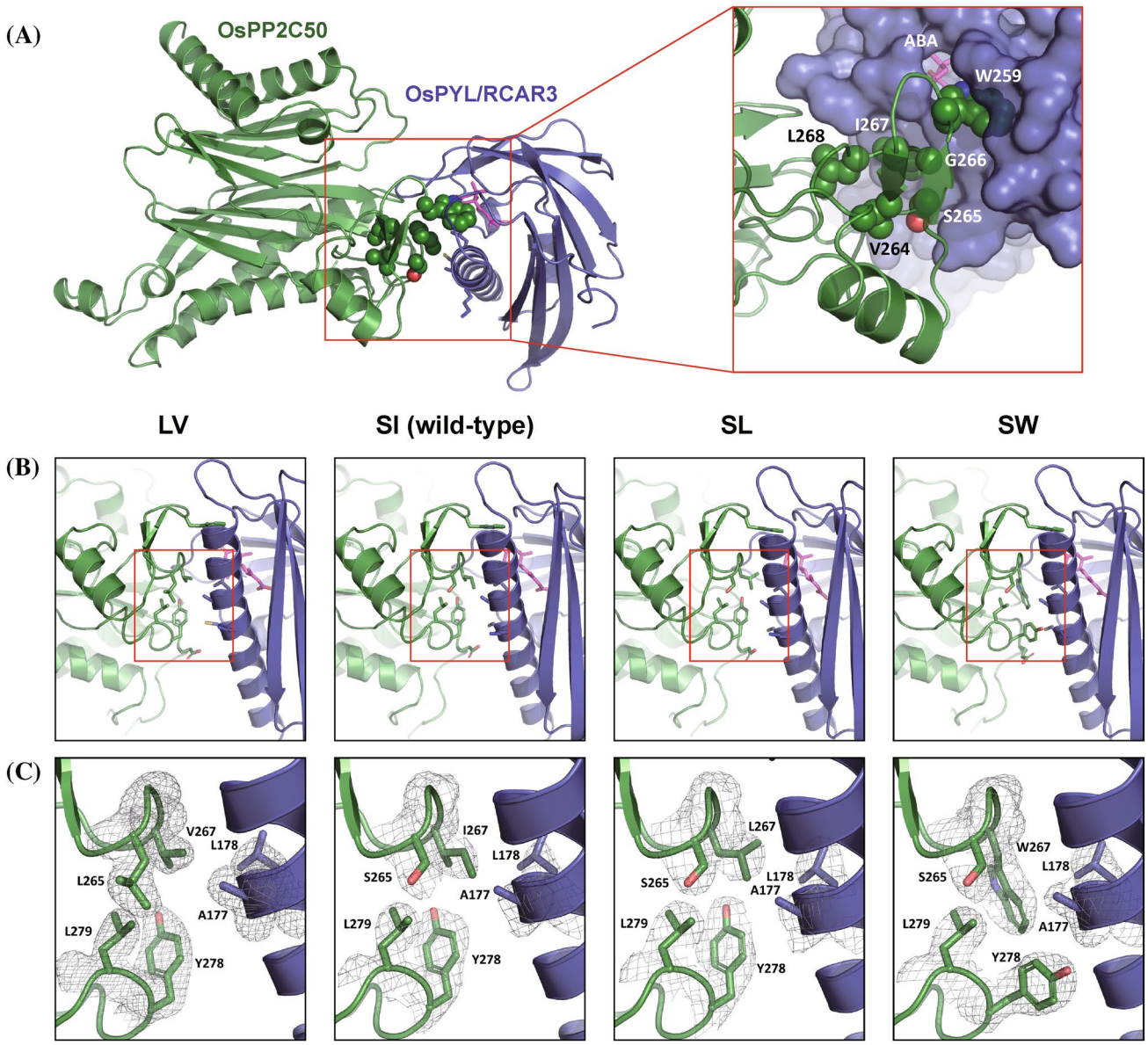

Fig. 2 Comparison of the interface between OsPP2C50 VxGΦL motif mutants and OsPYL/RCAR3. **a** Overall structure of OsPP2C50 wild-type (green):ABA (magenta):OsPYL/RCAR3 (blue) (PDB ID: 5GWP). The inset shows the interface between OsPP2C50 and OsPYL/RCAR3. Red boxes indicate the position where the VxGΦL motifs are. Key interface residues of OsPP2C50, including the wedging tryptophan (W259) and the VxGΦL motif residues (^{264}VSGIL^{268}), are described as sphere representations. **b** OsPP2C50:OsPYL/RCAR3 interface centered on the VxGΦL motif from the crystal structures of three OsPP2C50 mutants (labeled as LV, SL and SW). LV, SI, SL and SW indicate the amino acid identities in the second and fourth positions in the VxGΦL motif of OsPP2C50. LV corresponds to the canonical residues of the VxGΦL motif. SI indicates the wild-type of OsPP2C50 from the previously determined crystal structure (PDB ID: 5GWP). **c** Electron densities of residues near the VxGΦL motif. Omit map is contoured at 1 σ. In panels (**a**) through (**c**), one letter amino acid code is used and ABA (magenta) is depicted as stick representations. In panels (**b**) and (**c**), side chains of residues from OsPP2C50 are described as green stick representations

reinforcing the idea that the size and hydrophobicity of the fourth position of the motif might be the key parameter for the energy score. In the SG mutant, reduced van der Waals force, weighted sum of Lennard-Jones attractive and repulsive energy terms between other residues (fa_atr and fa_rep) and Lennard-Jones repulsive energy term in the same residue (fa_intra_rep), is likely to be a major factor to lower the binding affinity to OsPYL/RCAR3 (Supplementary Table S3): − 3.50 REU (Rosetta energy unit) (SG) vs. − 7.93 (SI), − 9.02 (SF) and − 10.15 REU (SW). This reduced van der Waals force of the SG mutant of OsPP2C50 apparently contributes to losing the binding affinity to OsPYL/RCAR3,

Table 3 Crystallographic date collection and refinement statistics

	OsPP2C50:ABA:OsPYL/RCAR3		
OsPP2C50 mutant	S265L/I267V ("LV")	I267L ("SL")	I267W ("SW")
PDB ID	5ZCG	5ZCL	5ZCH
Data collection and processing			
Wavelength (Å)	0.9795	0.9795	0.9795
Resolution range (Å)	29.6–2.1 (2.175–2.1)[a]	37.53–2.661 (2.757–2.661)	24.71–2.474 (2.563–2.474)
Space group	*P1*	$P2_1$	*P1*
Unit cell (a, b, c, α, β, γ)	70.73, 76.35, 77.94, 62.96, 72.03, 66.93	75.09, 130.26, 80.25, 90, 115.99, 90	71.73, 76.02, 78.58, 62.29, 73.09, 65.01
Total reflections	240,859 (24281)	162,580 (14,371)	146,755 (13,240)
Unique reflections	74,164 (7413)	39,539 (3799)	45,783 (4238)
Multiplicity	3.2 (3.3)	4.1 (3.8)	3.2 (3.1)
Completeness (%)	93.39 (87.13)	99.27 (95.73)	96.87 (89.58)
Mean $I/\sigma(I)$	19.41 (4.60)	9.22 (1.78)	15.16 (2.43)
Wilson B factor	32.30	48.12	46.69
R_{merge}	0.0675 (0.3323)	0.1204 (0.708)	0.1047 (0.7723)
R_{meas}	0.08215 (0.4003)	0.1379 (0.8219)	0.1258 (0.9293)
$CC^{1/2}$	0.996 (0.912)	0.993 (0.648)	0.993 (0.593)
CC^*	0.999 (0.977)	0.998 (0.887)	0.998 (0.863)
Refinement			
R_{work}	0.2027 (0.2599)	0.1952 (0.2985)	0.2062 (0.2879)
R_{free}	0.2386 (0.3560)	0.2400 (0.3525)	0.2300 (0.3364)
CC_{work}	0.937 (0.883)	0.946 (0.785)	0.947 (0.785)
CC_{free}	0.916 (0.796)	0.942 (0.599)	0.919 (0.808)
No. of non-hydrogen atoms	7876	7390	7337
Macromolecules	7315	7276	7130
Ligands	42	42	42
Water	519	72	165
RMSD			
Bond length	0.005	0.005	0.004
Bond angle	1.06	0.71	1.06
Ramachandran			
Favored (%)	98.70	97.19	98.00
Allowed (%)	1.30	2.70	2.00
Dis-allowed (%)	0.00	0.11	0.00
Average B factor	42.73	50.45	55.54
Macromolecules	42.22	50.59	55.71
Ligands	33.91	40.63	48.66
Solvent	50.67	41.80	49.97

[a]Numbers in the highest resolution shell

evidenced by phosphatase inhibitory assay results (Fig. 1b, c). In the SF and SW mutants, increased internal energy of side-chain rotamer (fa_dun) due to bulky aromatic ring structure appears to be the culprit for reduced binding affinity to OsPYL/RCAR3 (Supplementary Fig. S2). The SF and SW mutants might suffer from spatial stress due to bulky side-chain sandwiched by OsPYL/RCAR3 and OsPP2C50. In line with the plausible destabilization of side-chain rotamers in the SF and SW mutants, conformational simulation of the SW mutant suggested that the most energy-favorable conformation of Trp267 caused van der Waals bumps by surroundings (Supplementary Fig. S3).

We further expanded energy analysis to serine and alanine variants used in BLI experiments (Fig. 3b). We found Lazaridis-Karplus solvation energy scores (fa_sol) of the hydrophilic mutants were relatively higher than those of hydrophobic mutants (SL, SF and SW mutants) as well as wild-type (Supplementary Fig. S2). For example, Solvation

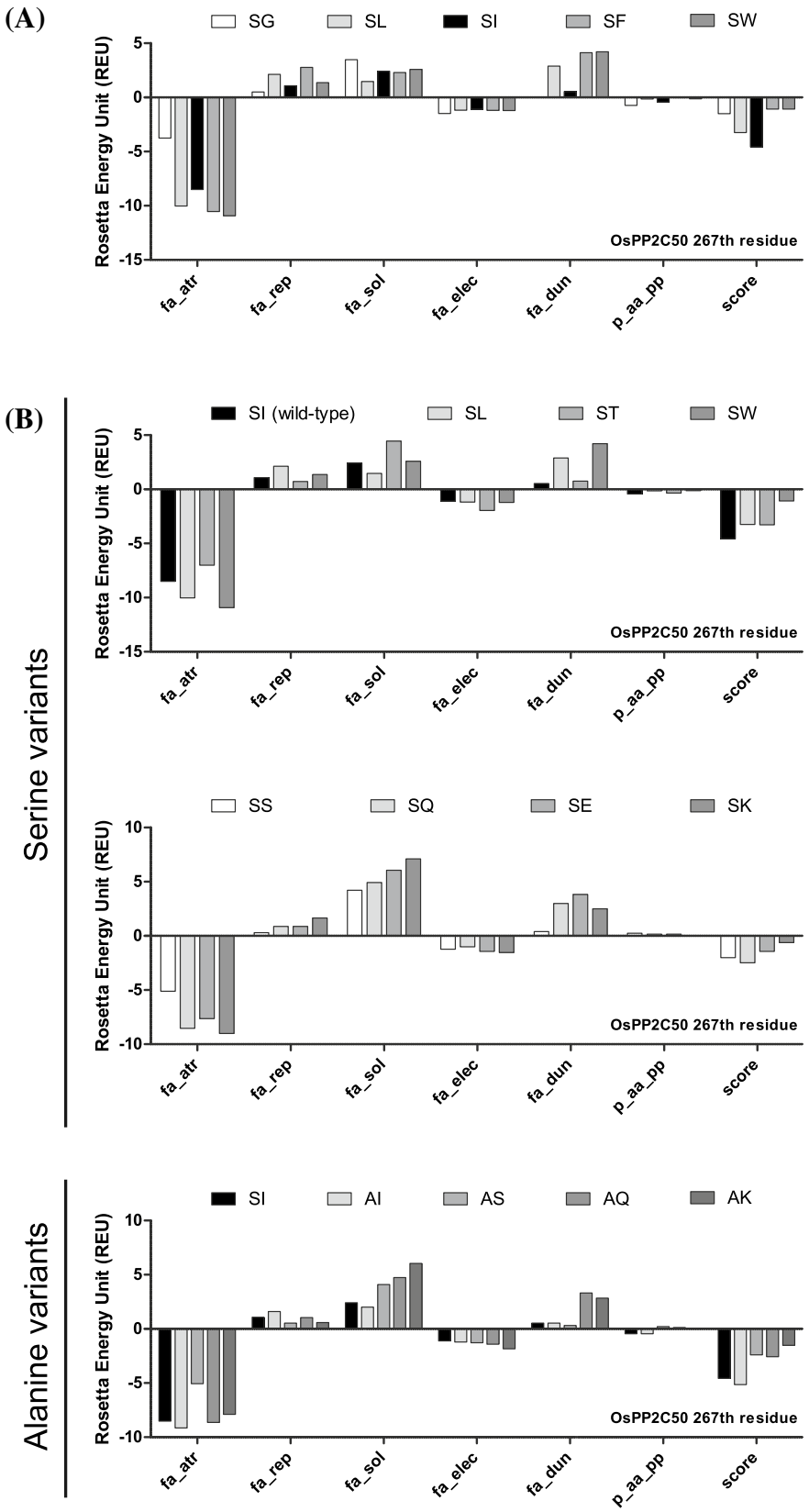

Fig. 3 Protein energy analysis on the motif involved in protein complex formation with hydrophobic or hydrophilic mutation. Protein energy scoring of residues in the fourth position of the VxGΦL motif. Per-residue energies of residues in the fourth position of the VxGΦL motif were calculated: **a** size-variable hydrophobic mutants and **b** serine and alanine variants generated by systematic mutagenesis in this study. 'SI' represents the OsPP2C50 wild-type and others the second and fourth residues of OsPP2C50 VxGΦL. Structure of OsPP2C50 mutants were generated and their energies were calculated by Relax protocol of Rosetta3 software with REF2015 score function. Details of REF2015 is described in Supplementary Table S3

energy score of the SQ mutant was twice as much as that of wild-type: 2.4 (SI) vs. 4.9 REU (SQ). Such an increase in solvation energy score of the SQ mutant apparently accounts for its lowered affinity (K_d values) to OsPYL/RCAR3 than the wild-type despite similar van der Waals force: 3.7 nM for wild-type versus 90 nM for SQ mutant (Table 1). In addition, the solvation energy scores increased in proportion to side-chain size of hydrophilic residues on 267th residue of OsPP2C50. These results with serine variants were also consistent with those with alanine variants. There was no much difference in energy scores between the wild-type (SI) and the AI mutant. From AI to AS, AQ and AK mutants, solvation energy scores increased, negatively affecting total energy score. Furthermore, the AQ and AK mutants, harboring side-chains longer than Cδ, presented internal energy stress of their rotamers (fa_dun), which was another factor contributing to increased total energy score and reduced binding affinities. Collectively, the analyses of energetics for the second and the fourth position of the VxGΦL motif corroborated that the fourth position of the VxGΦL motif was more critical to the complex formation than the second position, and that the larger hydrophobic residues on the fourth position was more detrimental to the complex formation due to rotamer energy stress with sequence alteration to hydrophilic or charged residues impairing the interaction due to solvation energy stress.

Overexpression of OsPP2C50 mutants modulate ABA responsiveness during seed germination and root growth

To corroborate how the aforementioned single residue change in the VxGΦL motif affected ABA-related phenotypes in planta, we generated *OsPP2C50-OX* transgenic *Arabidopsis* lines of its wild-type (SI) and the SL, AS, AQ and AK mutants. The alanine variants (AS, AQ and AK mutants) were employed to exclude any potential effect by the presence of hydrophilic serine in the second position. Two independent T_3 transgenic progenies of each mutant (SI-2, SI-3; SL-6, SL-7; AS-3, AS-14; AQ-1, AQ-2; and AK-10, AK-11) were selected for seed germination, root growth and gene expression analyses (Fig. 4). The SI and SL *Arabidopsis* lines showed similar level of germination rate to Col-0 in the presence of 0.5 µM ABA. These results were consistent with the in vitro observation that the binding affinities of OsPP2C50 wild-type and SL mutant to OsPYL/RCAR3 were very similar (Fig. 1b and Table 1). By contrast, the AS and AK *Arabidopsis* lines showed significantly increased germination rate in comparison to those of Col-0 and SI *Arabidopsis* lines (Fig. 4a). The AS transgenic *Arabidopsis* lines demonstrated no response to ABA in early seedling growth, judged by more green cotyledons than others (Fig. 4b). This observation suggests that overexpression of *OsPP2C50-OX* AS mutant might have suppressed ABA responsiveness in *Arabidopsis* in the presence of ABA despite its ninefold lower affinity to OsPYL/RCAR3 than the wild-type in vitro (Table 1). However, the AQ and AK mutant lines behaved similarly to Col-0 in early seedling growth although binding affinities of the AQ and AK mutants were much weaker than the AS mutant (Table 1). Primary root lengths of *OsPP2C50-OX* AS lines with ABA treatment were longer than without ABA, which was usually shorter in ABA treatment like Col-0 and other transgenic lines (Fig. 4c). The AQ and AK mutant lines exhibited primary root growth patterns very similar to those of Col-0, SI and SL mutant lines. Although we cannot account for these peculiar phenotypes caused by the AQ and AK mutants based on the in vitro binding data, it is plausible that sequence alteration of the fourth position of the VxGΦL motif to hydrophilic residues can modulate ABA responsiveness *in planta*. The *OsPP2C50-OX* AS mutant lines showed the lowest expression of ABA-inducible marker genes such as *RAB18* and *RD29B* with ABA treatment (Fig. 4d). High germination rate, high primary root growth and low expression rate of ABA-inducible marker genes indicated that ABA signaling network of the *OsPP2C50-OX* AS mutant lines was altered, leading to reduction of the signaling strength. We expected that *OsPP2C50-OX* AQ and AK mutant lines show the most significant alteration of ABA responsiveness based on the in vitro binding data. However, no noticeable alteration in the ABA signaling strength was observed for the *OsPP2C50-OX* AQ and AK mutant lines, suggesting that other factors might have been involved for presentation of phenotypes of these mutant lines. Our previous study revealed that alteration of the VxGΦL motif might impair the interaction with multiple biding partners involved in ABA signaling network, *e.g.* PYL/RCARs and SAPK10, a rice orthologue of *Arabidopsis* kinase OST1 (Han et al. 2017; Soon et al. 2012). Taken together, these results imply that the VxGΦL motif is a highly influential key motif to modulate ABA signaling strength exclusively via its fourth position.

Discussion

Clade A PP2C proteins serve as a signaling switch hub by interacting with PYL/RCARs or SnRK2 s competitively upon environmental abiotic stresses (Umezawa et al. 2010). We previously revealed that the VxGΦL motif of a PP2C is involved in interactions with components of the core ABA pathway, combined with the 'wedging tryptophan' inserted into binding clefts (Han et al. 2017). In this study, we provide more details on how the VxGΦL motif impacts on the PP2C:PYL/RCAR interaction via structural, biochemical and physiological approaches. As PP2C:PYL/RCAR3

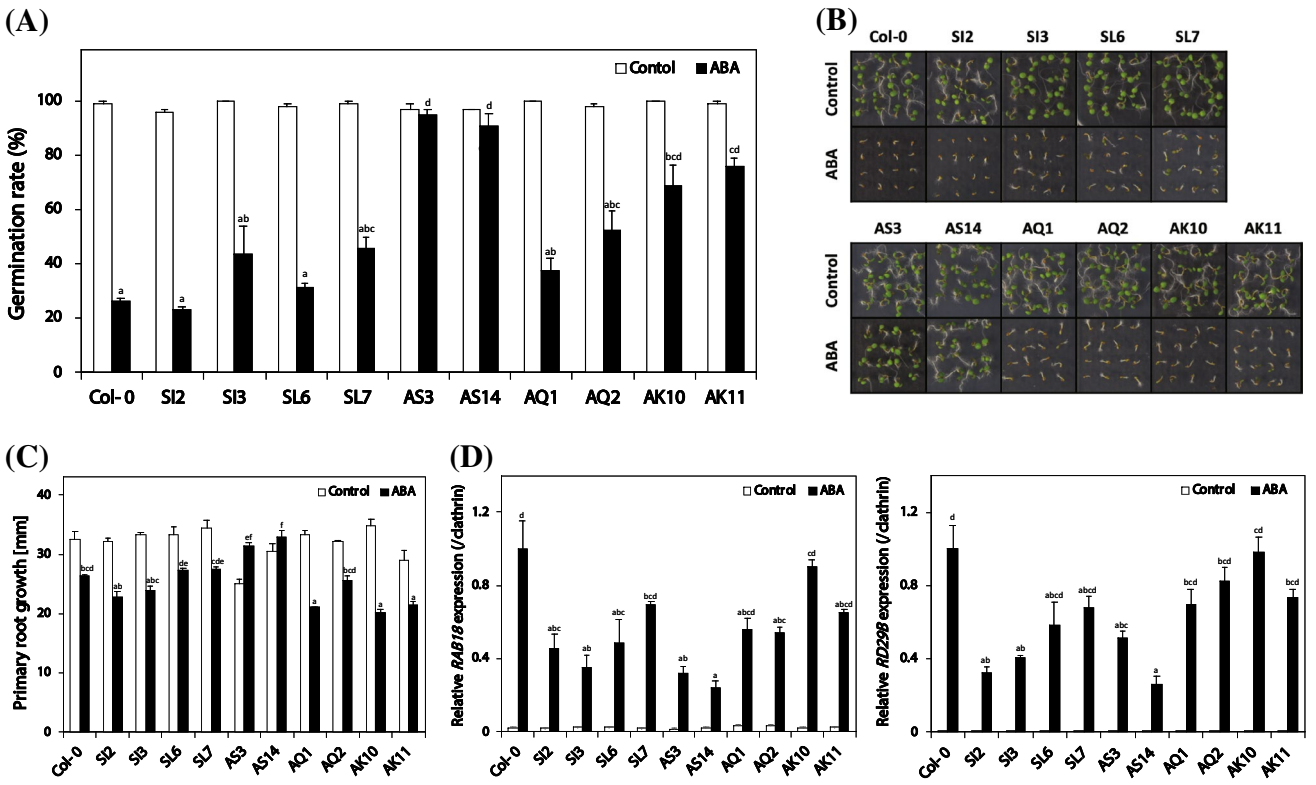

Fig. 4 Seed germination and gene expression analyses of OsPP2C50 mutants. **a** Seed germination rates of *OsPP2C50-OX* transgenic lines which were grown on the MS agar medium (0.5X) with 0.5 μM ABA or control medium. The number of seeds with visible radicles was counted at 4 days after vernalization. **b** Early seedling growths of *OsPP2C50-OX* transgenic lines used in **a** were photographed at 5 days after vernalization. **c** Primary root growths of *OsPP2C50-OX* transgenic lines in response to ABA. 10-day-old seedlings of each line vertically grown on normal medium were transferred to the MS agar medium (0.5X) with or without 10 μM ABA and then grown for 6 more days. **d** The ABA-induction of *RAB18* and *RD29B* expressions was measured by quantitative real-time PCR. Expression of clathrin gene was used as an internal control. 7-day-old seedlings of each *OsPP2C50-OX* line were treated with either 10 μM ABA or control solution for 6 h. The data in (**a**), (**c**) and (**d**) show mean ± SEM from three independent experiments. Different letters above the graph represent significant differences, ANOVA; $P < 0.01$

interaction is a trigger of ABA signaling pathway for abiotic stress tolerance in plants, we hypothesized that VxGΦL motif alterations could modulate ABA responsiveness of plants. We uncover that the fourth position of the motif is the most crucial and prefers aliphatic residues to aromatic and hydrophilic ones. Aliphatic residues contribute enough van der Waals forces to the binding interfaces, which consist of hydrophobic patches (Melcher et al. 2009; Soon et al. 2012; West et al. 2013; Yin et al. 2009). Large and bulky side chains, such as methionine or phenylalanine, can provide much more van der Waals force, but they turned out to be detrimental to interaction with their rotamers conferring spatial stress. Hydrophilic ones make the protein complex unstable because of their apolar interfaces. We introduced VxGΦL motif mutants of *OsPP2C50-OX* into *Arabidopsis* to observe that the AS and AK mutant lines could change ABA responsiveness *in planta*.

The fourth position of the VxGΦL motif, most critical in the interaction of OsPP2C50 with OsPYL/RCAR3, preferred aliphatic residues among clade A PP2Cs in plants including *Arabidopsis*, rice and corn (Supplementary Fig. S1). Consistent with this from multiple sequence alignment, we also obtained aliphatic mutants on the fourth position by directed evolution with no clear improvement in affinities (Tables 1 and 2). In silico mutagenesis searching for a better-affinity combination of the second and fourth positions of the VxGΦL motif yielded 'VMGIL' sequence with twofold worse experimental affinity toward OsPYL/RCAR3 (data not shown). These results implicate that mutational space of the VxGΦL motif is evolutionally saturated. Crystallographic and energetics analyses of the PP2C:PYL/RCAR complexes enabled us to propose how the aliphatic residues on the fourth position contribute to PP2C:PYL/RCAR complex stability. Multiple sequence alignment, directed evolution and crystallography analysis results strongly demonstrate that aliphatic residues such as valine and isoleucine are highly preferred in the fourth position of the motif (Supplementary Figs. S1, S2 and S3). Energetic analysis results

revealed that the OsPP2C50 motif mutants can be grouped to two using rotamer energy (fa_dun) as a criterion: (1): the SG, SI, SS and ST mutants having low rotamer energy (fa_dun < 1, average ~ 0.412) and (2) the SL, SF, SW, SQ, SE and SK mutants having high rotamer energy (fa_dun > 2, average ~ 3.4) (Supplementary Table S2). In the 'low rotamer energy' group, there are glycine, isoleucine, serine and threonine on their fourth positions of the VxGΦL motif. Glycine has no side-chain and serine only Cβ with carboxyl group. Isoleucine and threonine have slightly longer side-chains up to Cγ and Cδ, respectively, branching out from Cβ. They experience less spatial stress on interaction with OsPYL/RCAR3 by energy calculation results. In the 'high rotamer energy' group, however, there are much longer and aromatic residues, such as glutamine, lysine and phenylalanine. Glutamine and glutamic acid have up to Cδ on their side-chains, like isoleucine, but they are linear form, rather branched one. Isoleucine is more compact than glutamine and glutamic acid, plausibly conferring less rotameric stress at the interface of OsPP2C50 and OsPYL/RCAR3. The same reasoning can be applied to the SQ, SE, SK, AQ and AK mutants. Isoleucine and leucine have some common chemical features such as being hydrophobic, containing branched side-chains and featuring the same number of carbons in their side-chains. The only difference is where carbon chains are branched out: Cβ of isoleucine and Cγ of leucine. Such a subtle difference in branching-out position between isoleucine and leucine may possibly make the OsPP2C50 SL mutants experience more spatial stress, yielding ~ twofold weaker affinity to OsPYL/RCAR3 than the wild-type (SI) (Table 1). Aromatic residues, as in the OsPP2C50 SF and SW mutants, occupy much more space due to their ring structures. Such bulky structures are likely to cause unfavorable interactions with PYL/RCARs, which is reflected by the observation that the SW mutant showed ~ ninefold weaker affinity than the wild-type (Figs. 1b, c and 2). Moreover, aromatic residue was uncovered to cause van der Waals bumps between interfaces of PP2C and PYL/RCAR by our structural studies (Supplementary Fig. S3).

Hydrophobic effect in the VxGΦL motif, which refers to the formation of highly-ordered water cages around a hydrophobic patch onto protein surface, may play a key role in the PP2C:PYL/RCAR interaction (Tsai et al. 1997). Breakage of highly-ordered water cages in the hydrophobic residues, an energetically favored stage with higher entropy, would expose a hydrophobic interface of a protein to its binding partner. The VxGΦL motif might prefer hydrophobic residues to hydrophilic ones as they become stable close to hydrophobic patches onto PYL/RCAR interface. Water molecules surrounding a hydrophilic surface of a protein are relatively less ordered and make polar interactions with the hydrophilic surface, rendering exposition of hydrophilic residues in such an interface to the binding partner difficult. Since the VxGΦL motif is located in the hydrophobic environment, hydrophobic effect can be a major determinant for the preference of hydrophobic residues in the fourth position of the VxGΦL motif. Consistent with the aforementioned reasoning, our energetic analysis revealed that the hydrophilic residues in the VxGΦL motif experienced solvation energy stress (Fig. 3b).

Given that residues from both interacting proteins generally contribute to the interface, one would envisage that combination of mutations in both a PP2C and an ABA receptor could produce a "supercomplex" with higher affinity. Since we investigated thoroughly the residues on the PP2C side, we explored residues on the ABA receptor side. To identify residues that may be subject to mutation for the purpose of forming a "supercomplex", we analyzed the interface between OsPP2C50 and OsPYL/RCAR3 using PeptiDerive method of the Rosetta 3 suite (Sedan et al. 2016). The PeptiDerive module is designed to identify residues involved in the protein interaction by calculating interface energy of candidate residue(s). Analysis by the PeptiDerive revealed that the VxGΦL motif of OsPP2C50 was highly involved at the interface (data not shown), confirming our results by structural and biochemical analyses. Two regions of OsPYL/RCAR3 were predicted to be involved in the interaction: (1) residues from 97th to 106th and (2) 169th–178th (Supplementary Fig. S4A). The first region is the highly conserved 'gate loop' known to be crucial for ABA recognition (Melcher et al. 2009; Yin et al. 2009). Considering the evolutionary conservation of the sequence of the first region and its established role in binding to ABA, any mutation of residues in this region is likely to induce a negative effect on ABA recognition. Interestingly, the second region faces the VxGΦL motif of OsPP2C50 (Supplementary Fig. S4B and C). Multiple sequence alignment of the second region of ABA receptors in rice and Arabidopsis revealed two non-conserved residues that might be subject to directed evolution to possibly enhance binding affinity with OsPP2C50: Y173 and A177 of OsPYL/RCAR3 (Supplementary Fig. S4D). D169 and E170 are highly conserved as negatively charged one and involved in ion-ion interactions (Supplementary Fig. S4D) (Han et al. 2017). C173 is relatively less conserved, but keeps protein stability via intramolecular disulfide bond. F174 is involved in π-π interaction with W259 of OsPP2C50. L178 is also highly conserved as leucine and valine and involved in ABA or pyrabactin recognition (Han et al. 2017; Melcher et al. 2009, 2010; Yin et al. 2009; Yuan et al. 2010). As we suggest, the combination of mutations on Y173 and 177 of PYL/RCAR3, where faces the VxGΦL motif of Clade A PP2C proteins, could possibly impose ABA-hypersensitivity of plants via forming the "supercomplex".

Acknowledgements We thank the staff members at beamline 5C, Pohang Accelerator Laboratory for technical assistance in crystallographic data collection. This work was supported by the Next-Generation BioGreen 21 program (PJ01367602) through the Rural Development Agency and the Basic Science Research Program (NRF-2017R1D1A1B03032185, NRF-2018R1A2B6004367 and NRF-2019R1A6A7076041) and the Science Research Center Program (SRC-2017R1A5A1014560) through the National Research Foundation of Korea (NRF) Grants. Accession numbers: Diffraction data and coordinates have been deposited to the protein data bank with accession numbers 5ZCG (LV mutant), 5ZCL (SL mutant) and 5ZCH (SW mutant). The accession number of the wild-type structure is 5GWP.

Author contributions SL conceived research plans and supervised experiments. SH designed, performed most of the experiments and analyzed the data. JL, YL and THK performed some experiments and analyzed the data. SH, THK and SL wrote the article with contributions from all the authors.

References

Adams PD et al (2010) PHENIX: a comprehensive Python-based system for macromolecular structure solution. Acta Crystallogr D Biol Crystallogr 66(2):213–221. https://doi.org/10.1107/s0907444909052925

Clough SJ, Bent AF (1998) Floral dip: a simplified method for *Agrobacterium*-mediated transformation of *Arabidopsis thaliana*. Plant J 16:735–743

Conway P, Tyka MD, DiMaio F, Konerding DE, Baker D (2014) Relaxation of backbone bond geometry improves protein energy landscape modeling. Protein Sci 23:47–55. https://doi.org/10.1002/pro.2389

Cutler SR, Rodriguez PL, Finkelstein RR, Abrams SR (2010) Abscisic acid: emergence of a core signaling network. Annu Rev Plant Biol 61:651–679

Dupeux F et al (2011) Modulation of abscisic acid signaling in vivo by an engineered receptor-insensitive protein phosphatase type 2C allele. Plant Physiol 156(1):106–116. https://doi.org/10.1104/pp.110.170894

Emsley P, Cowtan K (2004) Coot: model-building tools for molecular graphics. Acta Crystallogr D 60(12):2126–2132. https://doi.org/10.1107/s0907444904019158

Finkelstein R (2013) Abscisic Acid synthesis and response Arabidopsis Book. American Society of Plant Biologists, Rockville, p e0166

Han S et al (2017) Modulation of ABA signaling by altering VxGPhiL motif of PP2Cs in *Oryza sativa*. Mol Plant 10(9):1190–1205. https://doi.org/10.1016/j.molp.2017.08.003

Kim H et al (2012) A rice orthologue of the ABA receptor, OsPYL/RCAR5, is a positive regulator of the ABA signal transduction pathway in seed germination and early seedling growth. J Exp Bot 63(2):1013–1024. https://doi.org/10.1093/jxb/err338

Melcher K et al (2009) A gate-latch-lock mechanism for hormone signalling by abscisic acid receptors. Nature 462:602–608. https://doi.org/10.1038/nature08613

Melcher K et al (2010) Identification and mechanism of ABA receptor antagonism. Nat Struct Mol Biol 17:1102–1108. https://doi.org/10.1038/nsmb.1887

Ng LM et al (2011) Structural basis for basal activity and autoactivation of abscisic acid (ABA) signaling SnRK2 kinases. Proc Natl Acad Sci USA 108(52):21259–21264. https://doi.org/10.1073/pnas.1118651109

O'Meara MJ et al (2015) Combined covalent-electrostatic model of hydrogen bonding improves structure prediction with Rosetta. J Chem Theory Comput 11:609–622. https://doi.org/10.1021/ct500864r

Otwinowski Z, Minor W (1997) Processing of X-ray diffraction data collected in oscillation mode. Methods in enzymology. Academic Press, Cambridge, pp 307–326. https://doi.org/10.1016/S0076-6879(97)76066-X

Qi X, Sun Y, Xiong S (2015) A single freeze-thawing cycle for highly efficient solubilization of inclusion body proteins and its refolding into bioactive form. Microb Cell Fact 14:24. https://doi.org/10.1186/s12934-015-0208-6

Rabbani MA et al (2003) Monitoring expression profiles of rice genes under cold, drought, and high-salinity stresses and abscisic acid application using cDNA microarray and RNA gel-blot analyses. Plant Physiol 133(4):1755–1767. https://doi.org/10.1104/pp.103.025742

Saez A, Apostolova N, Gonzalez-Guzman M, Gonzalez-Garcia MP, Nicolas C, Lorenzo O, Rodriguez PL (2004) Gain-of-function and loss-of-function phenotypes of the protein phosphatase 2C HAB1 reveal its role as a negative regulator of abscisic acid signalling. Plant J 37(3):354–369

Sedan Y, Marcu O, Lyskov S, Schueler-Furman O (2016) Peptiderive server: derive peptide inhibitors from protein–protein interactions. Nucleic Acids Res 44:W536–W541. https://doi.org/10.1093/nar/gkw385

Seki M et al (2002) Monitoring the expression pattern of around 7,000 Arabidopsis genes under ABA treatments using a full-length cDNA microarray. Funct Integr Genomics 2(6):282–291. https://doi.org/10.1007/s10142-002-0070-6

Soon FF et al (2012) Molecular mimicry regulates ABA signaling by SnRK2 kinases and PP2C phosphatases. Science 335(6064):85–88. https://doi.org/10.1126/science.1215106

Tischer SV, Wunschel C, Papacek M, Kleigrewe K, Hofmann T, Christmann A, Grill E (2017) Combinatorial interaction network of abscisic acid receptors and coreceptors from *Arabidopsis thaliana*. Proc Natl Acad Sci USA 114:10280–10285. https://doi.org/10.1073/pnas.1706593114

Tsai CJ, Lin SL, Wolfson HJ, Nussinov R (1997) Studies of protein–protein interfaces: a statistical analysis of the hydrophobic effect. Protein Sci 6:53–64. https://doi.org/10.1002/pro.5560060106

Umezawa T, Nakashima K, Miyakawa T, Kuromori T, Tanokura M, Shinozaki K, Yamaguchi-Shinozaki K (2010) Molecular basis of the core regulatory network in ABA responses: sensing, signaling and transport. Plant Cell Physiol 51(11):1821–1839. https://doi.org/10.1093/pcp/pcq156

Vlad F et al (2009) Protein phosphatases 2C regulate the activation of the Snf1-related kinase OST1 by abscisic acid in Arabidopsis. Plant Cell 21(10):3170–3184. https://doi.org/10.1105/tpc.109.069179

West GM et al (2013) Protein conformation ensembles monitored by HDX reveal a structural rationale for abscisic acid signaling protein affinities and activities. Structure 21:229–235. https://doi.org/10.1016/j.str.2012.12.001

Yin P et al (2009) Structural insights into the mechanism of abscisic acid signaling by PYL proteins. Nat Struct Mol Biol 16:1230–1236. https://doi.org/10.1038/nsmb.1730

Yuan X, Yin P, Hao Q, Yan C, Wang J, Yan N (2010) Single amino acid alteration between valine and isoleucine determines the distinct pyrabactin selectivity by PYL1 and PYL2. J Biol Chem 285(37):28953–28958. https://doi.org/10.1074/jbc.m110.160192

Zhou XE et al (2012) Catalytic mechanism and kinase interactions of ABA-signaling PP2C phosphatases. Plant Signal Behav 7(5):581–588. https://doi.org/10.4161/psb.19694